J Appl Electrochem (2010) 40:175–190
DOI 10.1007/s10800-009-9993-0

ORIGINAL PAPER

Deposition of nanostructurated gold on *n*-doped silicon substrate by different electrochemical methods

M. Gamero · C. Alonso

Received: 9 March 2009 / Accepted: 16 August 2009 / Published online: 28 August 2009

Abstract A study has been performed to select optimum process conditions (temperature, pH, reagent concentration, reaction kinetics, deposition time, etc.) in gold deposition on Si(*n*) from sulphite/thiosulphate electrolytic baths. Gold deposits have been obtained by electrochemical techniques such as constant potential, constant current, cyclic voltammetry and pulsating overpotential, in diffusional regime or by charge transfer control, at two pH values (6 and 9) and two temperatures (30 and 50 °C). The surface morphology of the Au deposits was studied by scanning electron microscopy (SEM), the preferred orientation and average size of the Au electrodeposited particles on *n*-Si substrates were obtained by X-ray diffraction (XRD), and qualitative and semiquantitative analysis of the gold sample was performed by energy dispersive X-ray (EDX) and X-ray photoelectron spectroscopy (XPS). The surface sulphur content was much lower or almost zero for gold samples obtained at pH 9 compared to those obtained at pH 6. However, when the different methods were compared at pH 6, both cyclic voltammetry and pulsating overpotential deposition led to deposits with a low or zero sulphur content. The results also show that various morphologies with different grain sizes can be obtained without the addition of additives.

Keywords Gold · Silicon · Cyclic voltammetry · Overpotential deposition · Rotating disc electrode (RDE) · Quartz crystal microbalance (QCM)

M. Gamero · C. Alonso (✉)
Universidad Autónoma de Madrid, C/Tomás y Valiente 7, Cantoblanco, 28049 Madrid, Spain
e-mail: concepcion.alonso@uam.es

1 Introduction

Macroporous materials have attracted great attention in recent decades due to their potential for application in many areas such as catalysis [1], chemical sensors [2] and photonic crystals [3]. Within nanostructured materials, there is great interest in gold periodic metallic structures as new supports for biorecognition reactions and their application in biosensor development. Although electrodeposition is not much used in the infiltration of interstitial spaces between template spheres, it has significant advantages such as its low cost, low-temperature working conditions and precise control over the thickness and composition of the electrogenerated material. Until now, the electrolytic baths used for the preparation of gold films with regular submicron spherical holes arranged in a close-packed structure have been commercial baths [4]. However, the presence of additives in these baths and impurities in the resulting gold metal deposit makes them undesirable for application in biosensor development. Thus, it is necessary to use electrolytic baths without additives and obtain gold deposits free of impurities such as sulphur.

In the first place, explain briefly what the state of the art of this topic. The use of Au(I) sulphite complex for electrodepositing gold has been known since 1842 [5], and continues to be the most widely used gold complex for preparing non-cyanided baths. The sulphite bath without stabilising additives is unstable when operating at pH < 8, due mainly to the formation of colloidal gold appearing after the Au(I) species disproportion reaction.

In order to avoid this reaction, all commercial baths contain stabilising additives. The addition of a polyamide such as ethylenediamine is known to stabilise the bath by the formation of a mixed gold complex [5, 6] making it possible to operate at a lower pH, between 5 and 8.

Morrissey [7] discovered that the simultaneous addition of ethylenediamine and nitrobenzene stabilises the bath to the point that it can operate in a pH range between 4 and 6.5. Honma and Kagaya [8] used 2, 2-bipyridine as a stabiliser due to the formation of a complex with Au^{+}, largely eliminating the disproportion reaction.

The electrodeposition of gold from a Au(I) thiosulphate complex has been known since 1913 [6] but has never been put to a practical use. Given that the stability constant of the $[Au(S_2O_3)_2]^{3-}$ $K = 10^{26}$ complex is several orders of magnitude greater than that of the sulphite complex ($K = 10^{10}$), the thiosulphate bath could be expected to be a viable alternative to the sulphite complex. However, these baths are unstable at acid or neutral pH due to the disproportion reaction that thiosulphate ions experience to yield colloidal sulphur.

Subsequently, a gold electrolytic bath that contains Au(I)-thiosulphate complex and iodide ions as an additive was used. In this system, metallic gold is used as an anode. The quantities of gold dissolved from the anode during the deposition maintain a constant Au concentration in the bath [9].

More recently, Osaka et al. [10] have proposed the use of a gold plating bath containing sulphite and thiosulphate as ligands at pH 6, obtaining columnar Au deposits by means of a constant current density of 5 mA cm^{-2}. The gold deposits contain element sulphur as an impurity. Surprisingly, the sulphur content decreases as the total ligand concentration rises ($[S_2O_3{}^{2-}] + [SO_3{}^{2-}]$). In order to explain this fact the authors propose a mechanism for low ligand concentrations which implies the existence of an adsorbed intermediate ($Au_2S_2O_3$) [11]. This mixed ligand bath has been investigated to electrodeposit gold for microelectronic and optoelectronic applications [12]. Recent studies of gold deposition on semiconductors such as silicon in cyanided baths at alkaline pH [13, 14], as well as for other types of baths like sulphite with thallium adatoms [15] or on *n*-GaAs [16], aim to shed light on the initial states of nucleation and growth. In the former case, deposition takes place by progressive nucleation and growth limited by diffusion of three-dimensional hemispheric islands. However, for most applications of metals on semiconductors, a high nucleus density is required and the nucleus size needs to be uniform. Thallium is known as a great grain size refiner in gold deposition since it modifies the phenomenon of nucleation and growth.

Despite the wide use of gold plating baths containing sulphite and thiosulphate, there continues to be a poor understanding of the deposition mechanism on Si(*n*) and of deposit characteristics, i.e. morphology, composition and grain size. In this respect, gold deposits have been obtained applying only one electrochemical technique: constant current [10]. In the investigation under this study, we explored the possibility of electrodepositing gold from a bath containing both thiosulphate and sulfite as complexing agents (pH 6 or 9 and $T = 30$ or 50 °C) on a *n*-doped silicon substrate by means of different electrochemical techniques (cyclic voltammetry, square wave potential pulse, step potential, and step current). The results obtained show that it is possible to obtain gold deposits with different morphologies and grain sizes, free of impurities, i.e. sulphur and without the addition of additives.

2 Experimental

2.1 Electrochemical cell

An electrochemical cell with a three-electrode setup was used [17]. A platinum counter electrode and a mercurous sulphate reference electrode (MSE) were used. The working electrode area (Si disc) exposed to the solution was constant ($\pi r^2 = 0.785$ cm^2). The experiments were performed in solutions thermostated at 30 and 50 °C ± 0.5 °C, and at pH 9 and 6. As a prior stage to any experiment, the solution was deaerated by bubbling nitrogen gas. The solution was properly maintained in a N_2 atmosphere.

2.2 Electrodes

The working electrode was *n*-Si (100) (doped with phosphorus, 10^{18} atoms cm^{-3}) with a thickness of 300 ± 25 μm and a resistivity of 0.7–1.4 Ω cm. The native oxide was removed with 1% vol. HF solution for 10 min and finally rinsed with ultrapure water (Millipore, 18.2 MΩ).

The gold rotating disc electrode (model 628-10, Metrom) was activated by cyclic voltammetry in H_2SO_4 0.5 M at 100 mV s^{-1}, obtaining the electrochemical area from the reduction of gold oxides.

2.3 Reagents and solutions

All the solutions were prepared with ultrapure water by means of a Millipore Milli-Q system (18.2 $M\Omega^{-1}$). The reagents used were: 99% dodecahydrated disodium acid phosphate for analysis (Merck); 98% sodium sulphate (Sigma-Aldrich); 99.5% pentahydrated sodium thiosulphate (Aldrich); 99% sodium tetrachloraurate (Johnson Matthey); and 97% sulphuric acid (Merck) to adjust the pH to a value of 6.

The concentrations of the solutions were as follows: 0.30 M Na_2HPO_4; 0.42 M Na_2SO_3; 0.42 M $Na_2S_2O_3$; 0.015 M $NaAuCl_4$.

2.3.1 Preparation of solution

The basic medium was generated with 0.30 M Na_2HPO_4 at 50 °C, after which 0.015 M $NaAuCl_4$ was added to yield a golden solution. One crystal of $Na_2S_2O_3$ was added and the solution turned orange. We continued to add $Na_2S_2O_3$ up to the desired concentration for 10 mL (0.42 M), and the solution experienced a progressive loss of colour until becoming colourless. We added 0.42 M Na_2SO_3, which is the reducing agent from Au(III) to Au(I), and in the presence of excess thiosulphate the complex $[Au(S_2O_3)_2]^{3-}$ was formed. In order to obtain pH 6, it was acidified with 2 M H_2SO_4.

2.4 Equipment

The electrochemical techniques were carried out using a P.A.R. function generator, mod. 175 Universal Programmer and a BRUKER potentiostat, mod. 310.

A Quartz Crystal Microbalance (QCM200; SRS) was used to measure the adsorption of each bath component on the gold electrode. QCM measurements were performed with AT-cut quartz crystals (5.0 MHz) of 25-mm diameter and Au electrodes deposited over a Ti adhesion layer (Maxtek Inc., Santa Fe Springs, CA). An asymmetric keyhole electrode seup was used, in which the circular electrode areas were 1.37 cm^2 (front side) and 0.317 cm^2 (back side). The quartz crystals were cleaned by immersion in piranha solution (H_2SO_4/H_2O_2; 3:1, v/v) for 2 min, followed by rinsing with ultrapure water and drying with nitrogen. The Crystal Holder was connected to the QCM25 Crystal Oscillator. The QCM probe was stabilised in air, obtaining a frequency value close to 5 MHz, after which it was immersed in ultrapure water thermostated at the testing temperature (30.0 ± 0.5 °C) with a thermostatic bath (Digiter 100, Selecta). The decrease in the resonance frequency on transfer from air to pure water is tabulated at 25° as 715 Hz. Finally, the QCM probe was immersed in the working solution.

The equipment used for the characterization of gold electrodeposits was a Philips XL30 Scanning Electron Microscope, coupled to the EDAX DE4i analyser. The phases present in the gold electrodeposits were determined by X-ray diffractometry (X'Pert PRO XRD, Panalytical) at a glancing angle of 1° using Cu K_α line generated at 40 mA, 45 kV. Start Position [°2theta] 30,0100; End Position [°2theta] 99,9900; Step Size [°2theta] 0,0200; Scan Step Time [s] 2,0000. In order to determine the composition of the samples and for their identification, the PDF-4^+ database (ICDD) was used. The measurement of width at half height ($W_{1/2}$) of each of the diffractogram peaks, for the determination of crystallite size, was performed with the X'Pert HighScore Plus program. The diffractometer works with the wavelength of copper, which is 1.5406 nm.

The composition at the surface was analysed using X-ray photoelectron spectroscopy (XPS). Photoelectron spectra were obtained with a VG Escalab 200R spectrometer equipped with a hemispherical electron analyser (pass energy of 50 eV) and a Mg $K\alpha$ ($h\nu = 1254.6$ eV, 1 eV = 1.6302×10^{-19} J) X-ray source, powered at 120 W. The kinetic energies of photoelectrons were measured using a hemispherical electron analyser working in the constant pass energy mode. The background pressure in the analysis chamber was kept below 2×10^{-8} mbar during data acquisition. The XPS data signals were taken in increments of 0.1 eV with dwell times of 50 ms. Binding energies were calibrated relative to the C 1 s peak at 284.9 eV. High resolution spectra envelopes were obtained by curve-fitting synthetic peak components using the software "*XPS peak*". The raw data were used with no preliminary smoothing. Symmetric Gaussian–Lorentzian product functions were used to approximate the line shapes of the fitting components. Atomic ratios were computed from experimental intensity ratios and normalised by atomic sensitivity factors [18].

3 Results and discussion

3.1 Electrochemical study

3.1.1 Voltammograms of Si(n) electrode in disodium acid phosphate

In the first place, the voltammograms were recorded for the *n*-Si(100) electrode in the background electrolyte of Na_2HPO_4 at two pH values (6 and 9) and two different temperatures (30 and 50 °C) between the stability limits of water. For potentials more anodic than 0.3 V/MSE (Fig. 1), the electrode oxidation takes place, and at potentials more cathodic than −1.35 V, the start of the hydrogen evolution reaction occurs. This value is approximately 350 mV more cathodic than the theoretic value ($E = -1.005$ V (MSE)) due to the overvoltage of the hydrogen evolution reaction on Si(*n*).

The effect of a 20 °C temperature increase implies an increase in the intensity of both processes. Table 1 shows the potential limits of hydrogen evolution (experimental and theoretic) and silicon oxide formation, revealing a broad potential range corresponding to the double layer region where there are no faradaic processes.

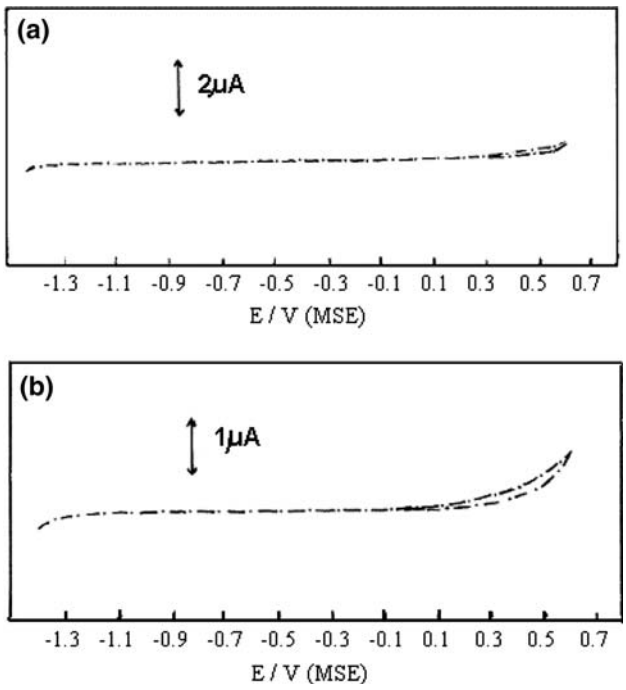

Fig. 1 Cyclic voltammogram of Si(*n*) electrode in Na_2HPO_4 solution. **a** pH = 6, $T = 30$ °C; **b** pH = 6, $T = 50$ °C ($v = 10$ mV/s). RE (MSE)

3.1.2 *Voltammograms of Si(n) electrode in electrolytic solution*

Figure 2 shows the voltammograms of the Si(*n*) electrode in the electrolytic bath. Bearing in mind the $Au(S_2O_3)_2^{3-}$ gold complex formation constant, from which it is supposed that the reduction takes place according to the following equation:

$$\left[Au(S_2O_3)_2\right]^{3-} + 1e^- \rightarrow Au^0 + 2(S_2O_3)^{2-} \quad (1)$$

it is possible to calculate the theoretic equilibrium potential for gold deposition:

$$\begin{aligned} E_{[Au(S_2O_3)_2]^{3-}/Au^0} &= E^0 + 2.3\frac{RT}{nF}\log\frac{\left[Au(S_2O_3)_2^{3-}\right]}{\left[Au^0\right]\left[(S_2O_3)^{2-}\right]^2} \\ &= E^0 + 2.3\frac{RT}{nF}\log K_f + 2.3\frac{RT}{nF}\log[Au^+] \\ &= +0.66 + 2.3\frac{RT}{nF}\log 10^{26} \\ &\quad + 2.3\frac{RT}{nF}\log 9.86 \times 10^{-28} \end{aligned}$$

where K_f is the complex formation constant. The Au^+ concentration is obtained supposing that the $[Au(S_2O_3)_2]^{3-}$ complex formation reaction is shifted in that direction, due to the high value of the constant. For a temperature of 30 °C the potential is $E = 0.599$ $V_{HNE} = -0.046$ V_{MSE} and for a temperature of 50 °C, $E = 0.596$ $V_{HNE} = -0.049$ V_{MSE}. This value is around one volt more positive than the theoretic value calculated for hydrogen evolution reaction (Table 1). Therefore, gold may be deposited without interference of the hydrogen evolution [19]. However, just as there is an overvoltage of hydrogen on Si(*n*), is experimentally observed a cathodic overvoltage around 0.8 V for gold deposition on Si, depending on the pH and the temperature (see Tafel table). Nevertheless, although the potential range is ostensibly reduced, gold deposits may be obtained without hydrogen interference between −0.8 V and the corresponding hydrogen limit.

Table 1 Potential limits of hydrogen evolution and SiO_2 formation

pH	T (°C)	E_{H_2} (V)$_{exp}$	E_{H_2} (V)$_{theoretic}$	E_{SiO_2} (V)
6	30	−1.350	−1.005	0.200
	50	−1.250	−1.029	−0.100
9	30	−1.500	−1.185	−0.250
	50	−1.400	−1.220	−0.600

A more detailed study of gold deposition on Si(*n*) shows two outstanding facts; the current in the anodic scan is always higher than in the cathodic scan, and the redissolution of gold is not observed (Fig. 2). The fact that Au deposition on Si is not observed at low potential (upd) is due to the weak interaction between the metal and the semiconductor. On the contrary, the observed nucleation overpotential of −0.8 V suggests that Au electrodeposition on Si(*n*) takes place preferentially on Au previously deposited on the silicon, as can be seen in the SEM micrographs (Fig. 7). When the substrate surface is partially covered, the gold deposit grows on existing nuclei and not on the free silicon surface, due to the fact that the Au–Si adsorption energy is lower than the Au–Au binding energy. The deposition of gold on gold becomes more evident in successive scans. Therefore, the area exposed for gold deposition is greater in the anodic scan than in the cathodic scan.

It should be pointed out that the initial potential for gold deposition after the first scan is around 0.2 V less negative, indicating that the overvoltage of gold deposition on gold (metal) is lower than on Si(*n*) (semiconductor), the latter having a high resistivity.

The second notable fact is that a stripping current is not observed on the anodic scan, indicating that the deposition of gold on Si(*n*) is an irreversible process. This is due to two effects: (1) the density of holes in the valence band is very low, and so the oxidation rate due to holes is very low (the holes receive the e^- of the metal when it oxidises); and (2) the height of the Si(*n*)/Au contact barrier is high, and thus gold cannot be oxidised since the energy barrier for

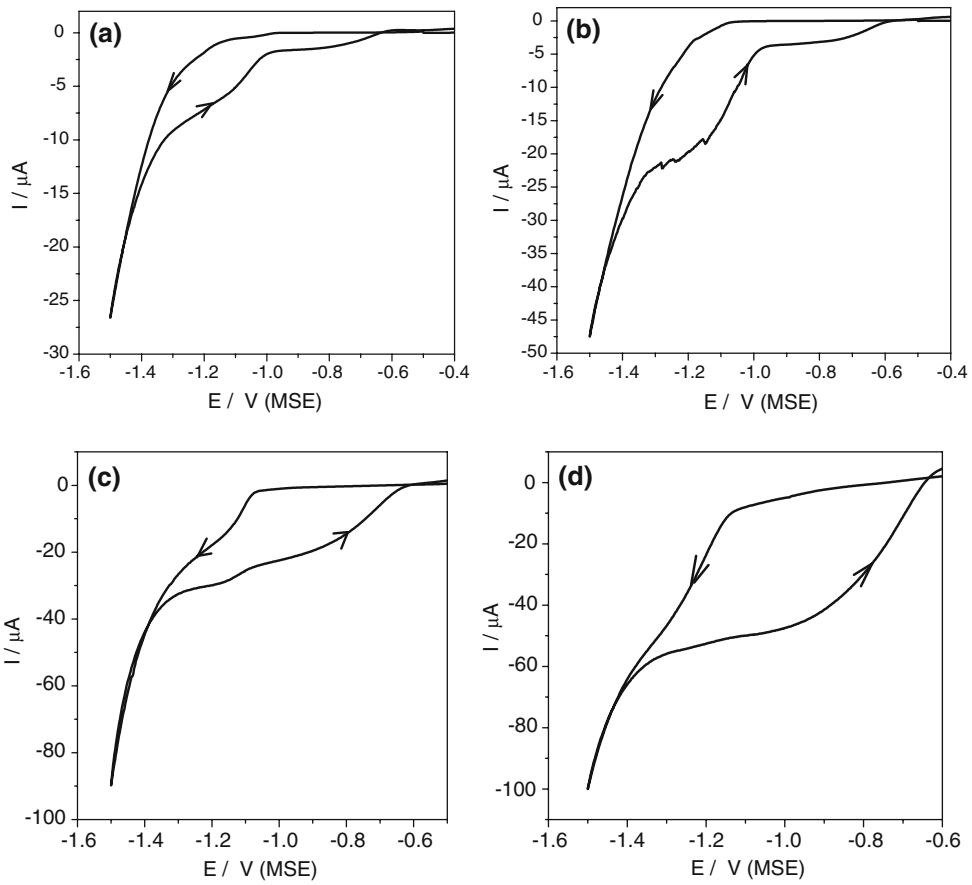

Fig. 2 CV of Si(*n*) electrode in solution of Na_2HPO_4 (0.30 M), Na_2SO_3 (0.42 M), $Na_2S_2O_3$ (0.42 M), $AuCl_4Na$ (0.015 M). **a** pH = 6, $T = 30$ °C; **b** pH = 6, $T = 50$ °C; **c** pH = 9, $T = 30°$; **d** pH = 9, $T = 50$ °C. $E_i = -0.6$ V, $E_f = -1.5$ V ($v = 10$ mV/s). RE (MSE))

electron transfer from gold to the conduction band is large [13, 14].

In general, irrespective of the pH and the temperature used, in the gold on Si deposition region the voltammograms show a current plateau in the forward scan and two plateaus in the reverse scan (Fig. 2). The appearance of a single plateau in the forward scan instead of two is due, on the one hand, to the great difference between the stability constants of the $[Au(S_2O_3)_2]^{3-}$ ($K = 10^{26}$) and $[Au(SO_3)_2]^{3-}$ ($K = 10^{10}$) complexes, so the reduction of gold takes place from $Au_2(S_2O_3)^{3-}$, and on the other hand the proportion of thiosulphate in relation to the gold concentration (30/1) used, causes that the second wave at more cathodic potentials, due to the reduction of gold from $Au_2(SO_3)^{3-}$, disappears obtaining a single plateau in all the potential range [10].

The final rise in current at the cathodic potential limit corresponds to the hydrogen development reaction (see Fig. 1), since the sulphite does not reduce on Si(*n*) at these potentials, unlike on Au, as shown in Fig. 4a.

If we observe the potentials at which the two plateaus appear in the reverse scan (Fig. 2), the first ($E < -1.0$ V for pH 6 and $E < 1.1$ V for pH 9) corresponds to the reduction of gold on Si(*n*) from the $[Au(S_2O_3)_2]^{3-}$ complex, as in the forward scan, and the second ($E > -1.0$ V for pH 6 and $E > 1.1$ V for pH 9) which takes place at a lower overvoltage, corresponds to the deposition of gold on previously deposited gold. The current plateau indicates that after nucleation, deposition is diffusion limited.

3.1.2.1 Tafel slopes In order to determine the reaction mechanism by which gold deposition on Si(*n*) takes place, Tafel slopes were determined at pH 6 and 9 and temperatures of 30 and 50 °C. For this purpose, voltammograms for Si(*n*) were recorded in the electrolytic solution between the potential limits of −0.6 and −1.6 V and a rate of 2 mV s^{-1}.

Table 2 sets out the values of the Tafel slopes obtained and the potential range where these have been calculated.

Table 2 The Tafel slope (*b*) and the potential range

pH	*T* (°C)	$E_{cathodic}$ (*V*)	E_{anodic} (*V*)	*b* (*V*)	$b(V)_{theoretic}$
6	30	−1. 00	−0.87	0.120	0.120
	50	−1.07	−0.94	0.136	0.128
9	30	−1. 08	−0.88	0.119	0.120
	50	−1.15	−0.99	0.125	0.128

From the results obtained it is deduced that the Tafel slope increases as the temperature rises, as predicted by the theoretic equation $2.3RT/\beta F$. The value of 120 mV corresponds to a step of charge transfer from an electron as a rate determining step. These values will subsequently be compared with the values calculated for gold deposition on gold. However, in principle it may be said that the mechanism of gold deposition on Si(n) seems to follow the same pattern as on gold, except for the overvoltage that needs to be exceeded for the reduction reaction to start. On the other hand it seems that the mechanism is not strongly dependent on the pH, but is favoured by a temperature increase.

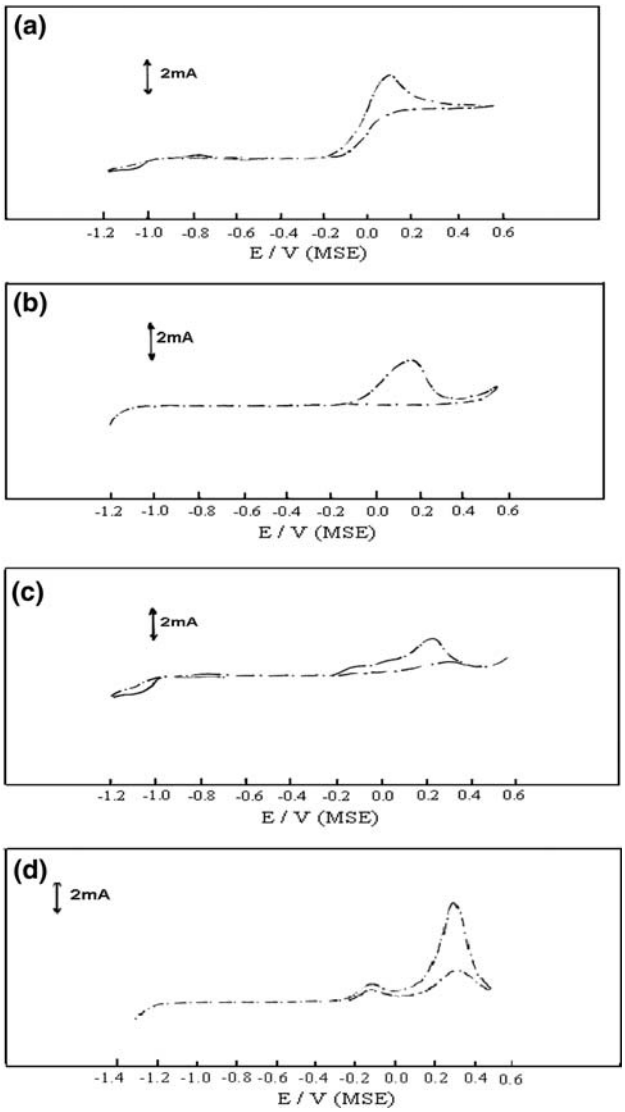

Fig. 3 Cyclic voltammogram of Au electrode in solution of Na_2HPO_4 (0.30 M). **a** pH = 6 Na_2SO_3 (0.42 M), **b** pH = 6 $Na_2S_2O_3$ (0.42 M), **c** pH = 6 Na_2SO_3 (0.42 M) + $Na_2S_2O_3$ (0.42 M), **d** pH = 9 Na_2SO_3 (0.42 M) + $Na_2S_2O_3$ (0.42 M). (v = 10 mV/s), T = 30 °C. RE (MSE)

3.1.3 *Voltammograms of Au electrode in disodium acid phosphate with $SO_3^{2-}/S_2O_3^{2-}$*

As we have just seen, and as the SEM images show, the electrochemical deposition of gold on Si(n) implies the deposition of gold on gold at low overpotentials. Figure 3 shows voltammograms corresponding to the gold electrode in sulphite (0.42 M) and thiosulphate (0.42 M).

For pH 9 the reduction reaction to hydrogen takes place at potentials more cathodic than −1.2 V. However, for pH 6, at potentials more cathodic than −1.0 V (T = 30 °C) or −0.9 V (T = 50 °C) a current plateau is observed in the cathodic scan and the corresponding oxidation peak in the anodic scan. The sulphite ion is liable to reduce to thiosulphate according to the following reaction:

$$2SO_3^{2-} + 6H^+ + 4e^- \rightarrow S_2O_3^{2-} + 3H_2O \quad (2)$$

being favoured at acid pH. In fact this peak does not appear at pH 9. Therefore, at this pH there will be no interference of a possible parallel reaction to gold deposition from the gold complex or complexes. It should be said that reduction of the sulphite does not take place on the Si(n) electrode.

3.1.4 *Voltammograms of Au electrode in electrolytic solution*

Figure 4 shows voltammograms for the gold electrode in the gold electrolytic bath. At pH 9 the deposition of gold on gold takes place in the forward scan, and hydrogen evolution occurs at potentials more cathodic than −1.2 V (voltammogram for gold in 0.30 M Na_2HPO_4 pH 9, T = 30 °C, image not shown). The initial potential, after which the reduction of Au^+ ions takes place, is around 300 mV less cathodic than for silicon, without reaching the theoretic value of −0.045 V for 30 °C (−0.049 V for 50 °C) (Table 3). Therefore, once gold starts to be deposited on silicon, subsequent deposition, which takes place on gold, can happen in a broader potential range, confirming what is seen in the second cycle of cyclic voltammogram of gold on Si(n).

In the reverse scan a current plateau is observed (−0.8 and −1.1 V) at similar potentials to the current plateau assigned as the deposition of gold on gold/Si(n) (Fig. 2). This current plateau indicates that the deposition of gold on the nuclei, at these potentials, is limited by ionic diffusion. According to the theory of nucleation and growth, it is known that metallic deposition at high cathodic overpotentials, i.e. when the charge transfer is fast, takes place preferentially on already formed nuclei, so that the metallic adatoms can subsequently diffuse towards more stable superficial sites.

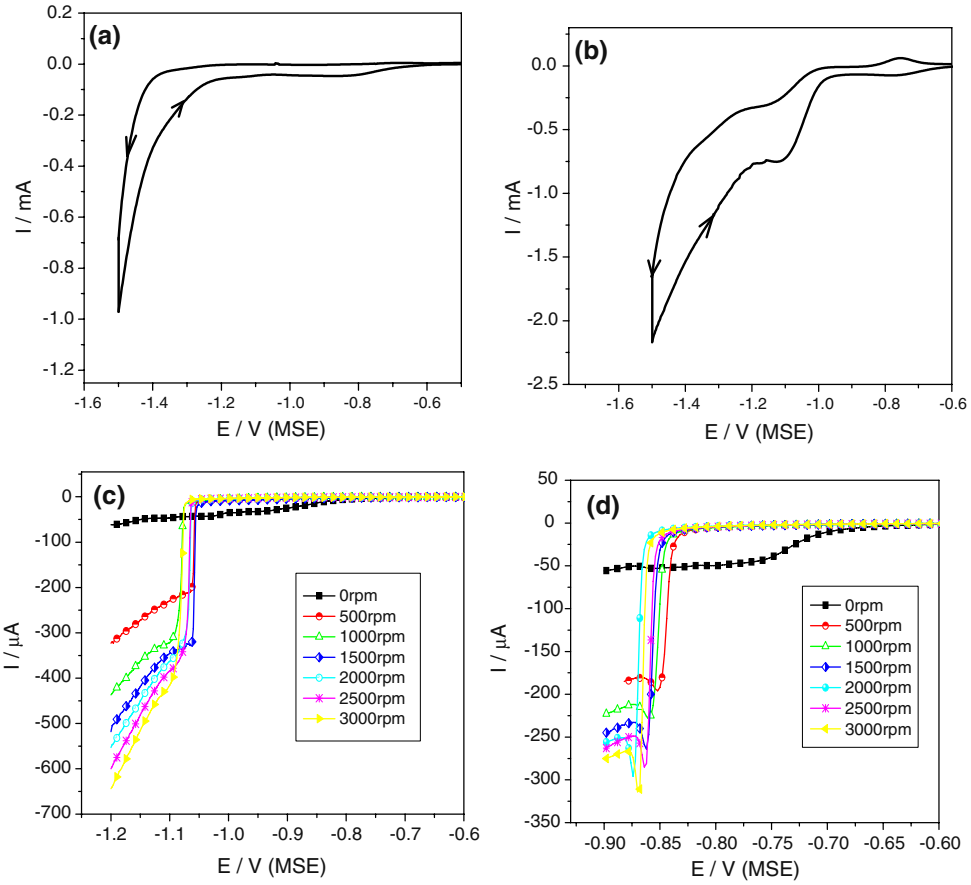

Fig. 4 Cyclic voltammogram of Au electrode in solution of Na_2HPO_4 (0.30 M) + Na_2SO_3 (0.42 M) + $Na_2S_2O_3$ (0.42 M) + $AuCl_4Na$: **a** pH = 9, T = 30 °C; **b** pH = 6, T = 30 °C (v = 10 mV/s); **c** *I*/*E* curve at different rotation rates ω, pH = 9, T = 50 °C (v = 2 mV/s); **d** *I*/*E* curve at different rotation rates ω. pH = 6 T = 50 °C (v = 2 mV/s). RE (MSE)

Table 3 The Tafel slope (b) and the potential range

pH	T (°C)	$E_{cathodic}$ (V)	E_{anodic} (V)	b (V)	b (V)$_{theoretic}$
9	30	−0.80	−0.60	0.125	0.120
	50	−0.86	−0.62	0.129	0.128
6	30	−0.72	−0.61	0.136	0.120
	50	−0.72	−0.58	0.140	0.128

For pH 6 the anodic scan of the voltammogram (Fig. 4b) shows a plateau for gold deposition (−0.75 and −1.0 V) and a second plateau (−1.0 and −1.2 V) for the reduction of sulphite ions to thiosulphate. This plateau is similar to that obtained for gold in a solution containing only sulphite ions (Fig. 3a). In fact, the same reduction peak can be seen in the cathodic scan. The current is greater in the anodic scan than in the cathodic scan, since the exposed area is greater in the anodic scan after gold has been deposited on gold in the cathodic scan.

3.1.4.1 Tafel slopes and measurements with EDR Tafel slopes were determined to compare the reaction mechanism for the reduction of $[Au(S_2O_3)_2]^{3-}$ ions on Si(n) with their reduction on Au. Use was made of a gold rotating disc electrode at zero rotation $\omega = 0$ and at the scanning rate (v = 2 mV s^{-1} (Fig. 4c, d). The values obtained and the potential range are shown in Table 3.

From the results obtained it is deduced that the Tafel slope increases as the temperature rises, as predicted by the theoretic equation $2.3RT/\beta F$. The value of 120 mV corresponds to an electron charge transfer step as the rate determining step.

$$\left[Au(S_2O_3)_2\right]^{3-} + 1e^- \rightarrow Au^0 + 2(S_2O_3)^{2-} \quad (3)$$

These values are similar to those previously obtained for Si(n), although the overvoltage for the reaction is lower. On the other hand, it seems that the mechanism is not strongly pH dependent, since the values are only slightly higher at pH 6 than at pH 9, indicating that the process would be more favoured at a mildly basic pH.

For pH 9, comparison of the voltammogram at $\omega = 0$ with the voltammograms recorded at higher rotation rates shows that the current density rises for potentials $E >$ −1.075 V, but remains at almost the same value for low polarization (Fig. 4c). In fact, in this potential region (−0.90 and −1.05 V) the current density decreases as the rotation rate rises ($\omega > 0$). Thus it may be concluded that the initial region of the voltammogram is defined by a slow charge transfer, where the Buttler-Volmer equation may be applied to calculate the Tafel slope, as in the preceding

section. Between this potential region and the current plateau there is a mixed charge transfer–mass transfer control and on the current plateau the gold deposition process is controlled by the diffusion of ions towards the electrode surface. These results are similar to those obtained for the Si(n) electrode, where the current plateau on the anodic scan (at low overvoltage) was attributed to gold deposition on gold nuclei previously deposited on Si(n) (Fig. 2).

Figure 4d shows I/E curves at different ω for pH 6. In this case the potential range where the current is greater for $\omega = 0$ than for higher rotation rates is broader than at pH 9, indicating that at this pH the transfer of electrons to reduce Au^+ ions from the $[Au(S_2O_3)_2]^{3-}$ complex to Au^0 is even slower. Furthermore, at pH 6, as ω increases so the start of the reduction curve shifts to more cathodic potentials.

Applying Levich's equation [20]

$$I_{\mathrm{lim,cat}} = 0.62\, nFD_0^{2/3} A\omega^{1/2} v^{-1/6} C_0$$

where D_0 is the diffusion coefficient; A the real electrode area; ω the electrode rotation rate; υ the kinematic viscosity (0.01 cm^2/s); C_0 the initial concentration in the solution (1.5×10^{-5} mol/cm^3 of Au^+); n the 1 exchanged electron.

Within the current plateau, where the process is controlled by ionic diffusion, a constant potential is selected and the current intensity is measured for each value of ω.

Table 4 Diffusion coefficient values

pH	(D_0/cm^2 s^{-1}) 30 °C	(D_0/cm^2 s^{-1}) 50 °C
6	1.87×10^{-5}	2.43×10^{-5}
9	3.45×10^{-5}	5.31×10^{-5}

A representation of the current intensity versus the square root of ω gives a straight line with a slope of $0.62\, nFD_0^{2/3} A v^{-1/6} C_0$, where all the terms are known, being possible to calculate the diffusion coefficient of $[Au(S_2O_3)_2]^{3-}$. Table 4 shows the values of the diffusion coefficient (D_0/cm^2 s^{-1}) for pH 6 and 9 and $T = 30$ °C and 50 °C. For each constant pH value, the diffusion coefficient rises with the temperature.

3.1.5 Quartz crystal microbalance (QCM)

The adsorption of each of the electrolyte bath components on a gold electrode was measured using a quartz crystal microbalance to discern the reaction mechanism for gold deposition i.e. whether it takes place in a single step, yielding sulphur-free electrodeposits; or in two steps, via an intermediate adsorbate, in which case it would give rise to deposits with a sulphur content. Assuming that the frequency decrease (Δf) is due to the change in mass arising from the adsorption of each of components present in the working solution, one can calculate Δm by applying Sauerbrey's equation [21].

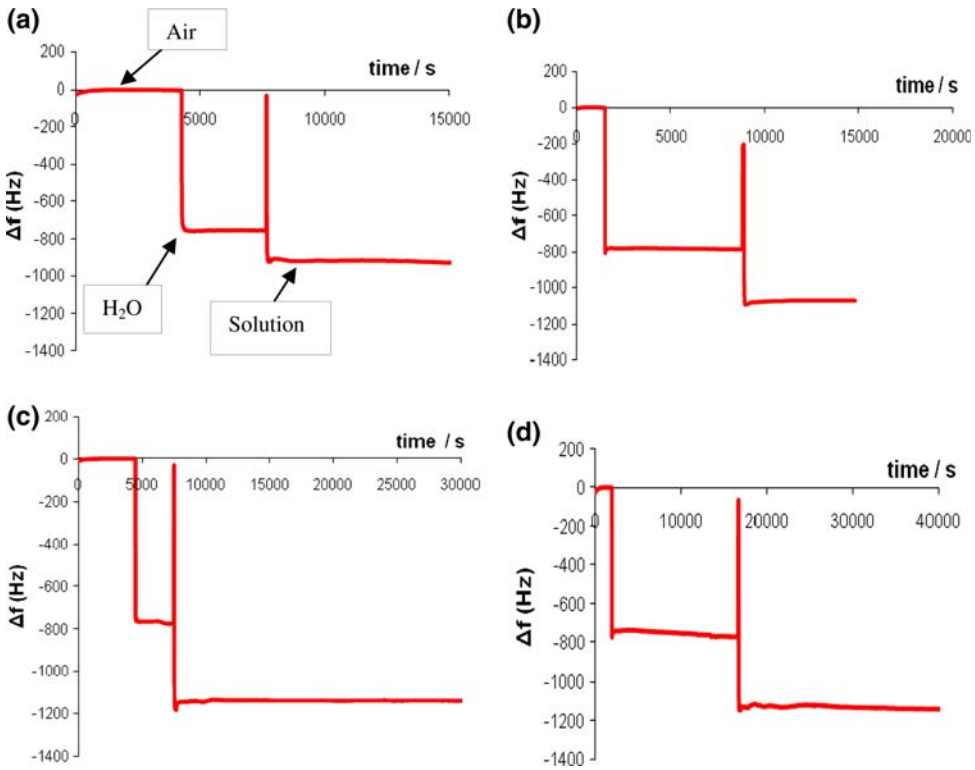

Fig. 5 Measurement of Δf with time for Au electrode in air(0), water and a solution of **a** Na_2HPO_4 (0.30 M); **b** Na_2HPO_4 (0.30 M) + Na_2SO_3 (0.42 M); **c** Na_2HPO_4 (0.30 M) + Na_2SO_3 (0.42 M) + $Na_2S_2O_3$ (0.42 M); **d** Na_2HPO_4 (0.30 M) + Na_2SO_3 (0.42 M) + $Na_2S_2O_3$ (0.42 M) + $AuCl_4Na$ (0.015 M). pH = 9, $T = 30$ °C

$$\Delta f = -C_f \Delta m$$

where Δf is the observed frequency change in Hz, Δm is the mass change (μg cm^{-2}) and C_f (56.6 μg^{-1} cm^2 Hz) is a proportionality constant for the 5.0 MHz crystals used in this study.

First of all the frequency change in time was measured for a background dissolution (Na_2PO_4H, pH 9) (Fig. 5a). The Δf obtained is 165 Hz and the corresponding increase in mass is $\Delta m = 2.91$ μg cm^{-2}, i.e. the $PO_4H_2^-$ ions are adsorbed on the gold electrode. If sodium sulphite is added in a concentration of 0.42 M, a drop of $\Delta f = 288$ Hz is obtained, of which 123 Hz correspond to the coadsorption of SO_3^{2-} ions. Therefore, SO_3^{2-} ions are adsorbed on the gold electrode (123 Hz and $\Delta m = 2.17$ μg cm^{-2}) (Fig. 5b). However, if the solution used is 0.30 M $PO_4H_2^-$ + 0.42 M SO_3^{2-} + 0.42 M $S_2O_3^{2-}$ the Δf is 374 Hz, and therefore thiosulphate ions are adsorbed in a lesser proportion than SO_3^{2-} ions ($\Delta m = 1.52$ μg cm^{-2}) (Fig. 5c). This same measurement performed in the presence of $NaAuCl_4$ does not show any additional negative frequency increase, indicating that there is no adsorbed reaction intermediate containing $S_2O_3^{2-}$ i.e. $(Au_2\ S_2O_3)_{ads}$ (Fig. 5d).

According to Osaka et al. [11], if the thiosulphate concentration is low in relation to the $[Au(S_2O_3)_2]^{3-}$ complex (7/1) the reaction mechanism consists of two steps; the first of them implies the adsorption of an $(Au_2\ S_2O_3)$ intermediate

$$2\left[Au(S_2O_3)_2\right]^{3-} \leftrightarrow (Au_2\ S_2O_3)_{ads} + 3\ S_2O_3^{2-} \quad (4)$$

$$(Au_2\ S_2O_3)_{ads} + 2e^- \rightarrow 2Au + S_2O_3^{2-} \quad (5)$$

$$\left[Au(S_2O_3)_2\right]^{3-} + e^- \rightarrow Au + 2\ S_2O_3^{2-} \quad (6)$$

The second reaction (5), as the rate determinant step, is an electrochemical reduction of $(Au_2\ S_2O_3)_{ads}$ to deposit gold

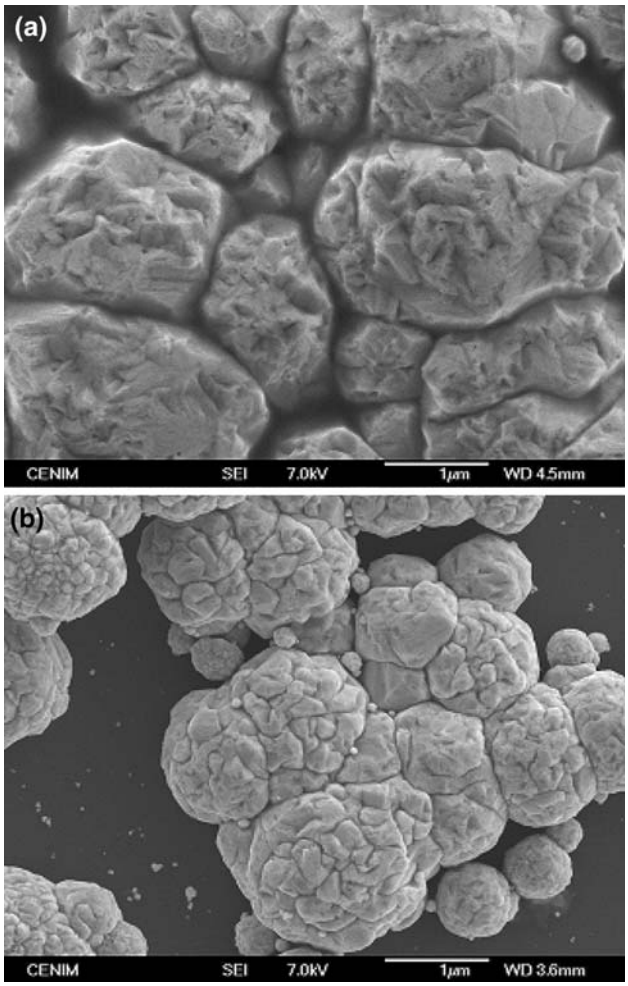

Fig. 6 Au bulk deposits on Si(*n*) obtained by cyclic voltammetry for 6 h. **a** $E_i = -0.80$ V, $E_f = -1.0$, pH = 9, $T = 30$ °C, Scale 1 μm. **b** $E_i = -0.80$ V, $E_f = -1.05$, pH = 9, $T = 50$ °C, Scale 1 μm. ($v = 10$ mV/s)

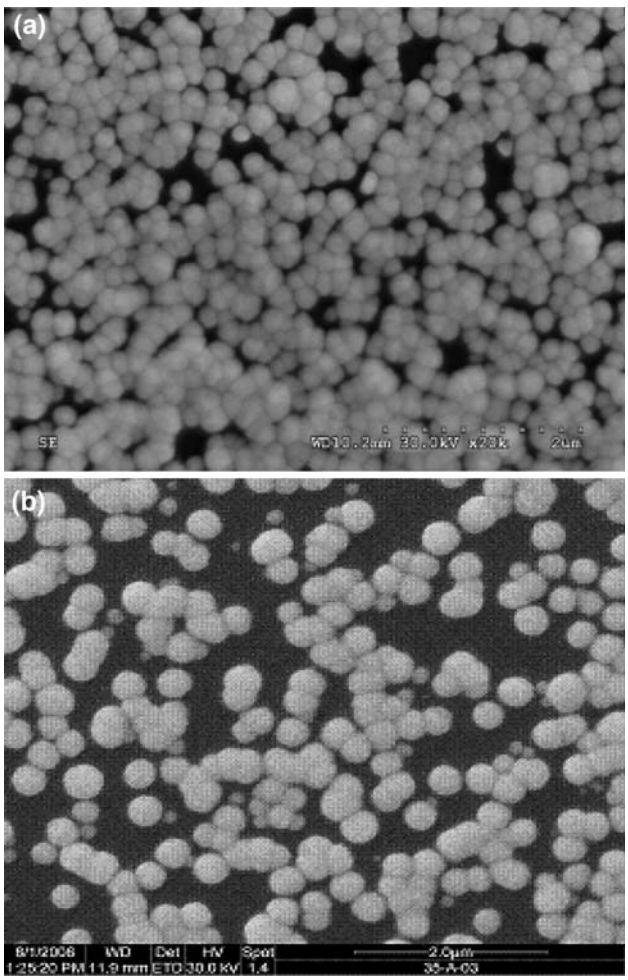

Fig. 7 Au bulk deposits on Si(*n*) obtained by cyclic voltammetry: **a** $E_i = -0.75$ V, $E_f = -1.65$ V. **b** $E_i = -0.75$ V, $E_f = -1.3$ V, pH = 9, $T = 30$ °C, Scale 2 μm ($v = 10$ mV/s)

with a global reaction given by reaction (6). In this case, the gold deposit contained sulphur. However, for high $S_2O_3^{2-}$ concentrations in relation to the $[Au(S_2O_3)_2]^{3-}$ complex (30/1), as in our case, the reaction (4) shifts towards the formation of the $[Au(S_2O_3)_2]^{3-}$ complex and gold deposition takes place directly from the species in solution without intermediates, following the reaction (6). In conclusion, the proposed mechanism for Au^+ reduction from the $[Au(S_2O_3)_2]^{3-}$ complex implies a charge transfer of $1e^-$ without adsorbed intermediates and therefore a sulphur-free gold deposit can be obtained.

3.2 Morphology of gold bulk deposits

The morphology of gold deposits on Si(*n*) obtained by different electrochemical techniques was observed by scanning electron microscopy (SEM). The composition of the deposits was determined by an energy dispersive X-ray (EDX) analyser coupled to the SEM and X-ray photoelectron spectroscopy (XPS). X-ray diffraction was used to determine the grain size of the gold deposits performed on the Si(*n*) substrate.

3.2.1 *Analysis by scanning electron microscopy (SEM)*

3.2.1.1 Cyclic voltammetry In view of the voltammograms obtained for gold deposition on Si (Fig. 2) and on gold (Fig. 4), it is possible to obtain deposits by applying potentials within the Tafel region (slow reduction reaction of Au^+ to Au^0) or in the potential range where this charge transfer is fast and the process is controlled by the diffusion of ions to the electrode surface. In this case cyclic voltammetry was applied in the Tafel region at a slow scanning rate ($v = 10$ mV s^{-1}) with the aim of obtaining a compact deposit. Figure 6a, b shows the SEM image for a

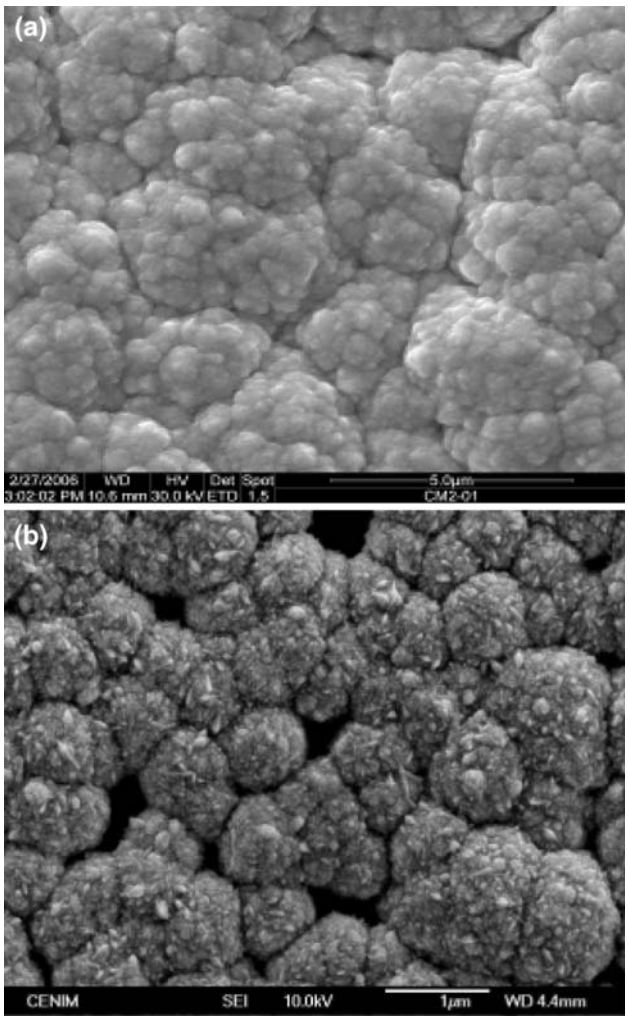

Fig. 8 Au bulk deposits on Si(*n*) obtained by constant potential: **a** $E_i = -1.1$ V, pH = 9, $T = 30$ °C, $t = 3$ h, Scale 5 μm. **b** $E_i = -1.0$ V, pH = 6, $T = 30$ °C, $t = 1$ h, Scale 1 μm

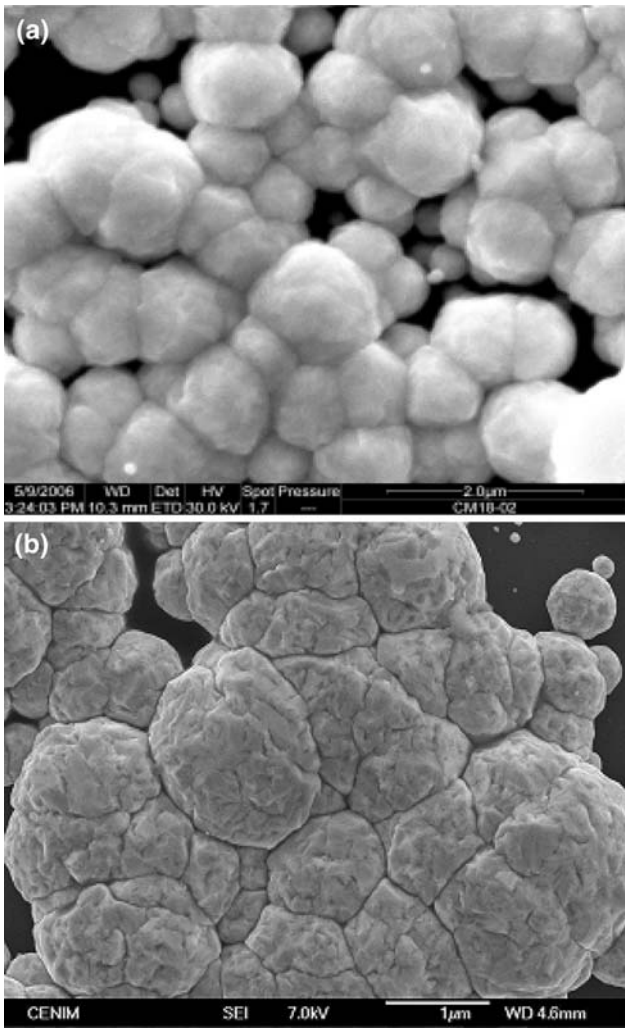

Fig. 9 Au bulk deposits on Si(*n*) obtained by constant current (CT): **a** $I = 7$ μA cm^{-2}, pH = 9, $T = 30$ °C, $t = 2$ h, Scale 2 μm. **b** $I = 5$ μA cm^{-2}, pH = 9, $T = 50$ °C, $t = 2$ h, Scale 1 μm

deposit obtained at pH 9. The silicon surface is only partly covered, despite the deposition time of six hours. As has previously been noted, after the first scan, gold deposits preferentially on the already deposited gold rather than on the free Si surface, since this requires a lower overvoltage, giving rise to 3D growth. The effect of a temperature increase causes each grain to appear smoother and more rounded, because the superficial diffusion of the adions increases with the temperature as well as the grain size (Table 6).

If the potential scan ends at potentials of more than −1.3 V, where the reduction reaction both on Si and on Au takes place under mass transfer control, the deposit obtained is uniform, formed of spherical particles whose grain size increases as the cathodic potential limit decreases (Fig. 7). In addition to the semiconducting nature of the substrate, metal electrodeposition on a semiconductor is also complicated by the nucleation process. The fact that the size of the nuclei is not uniform indicates that the nucleation process is progressive and not instantaneous, this being a disadvantage for most applications where a high nucleation density (it is obtained) and a uniform grain size are required. Due to the weak interaction between the metal and the semiconductor, nucleation of the metal follows Volmer-Weber's mechanism with the formation of islands and a 3D growth process, controlled by the transport of ions to the interface [22, 23].

3.2.1.2 Constant potential To our knowledge no morphological study has been reported on the structure of gold deposits performed at constant potential on Si(*n*) from sulphite/thiosulphate baths, except for the study by Huang et al. [15] on the first stages of nucleation and growth from current transients applying the theory of Scharifker [23]. In our case, the deposits have been performed imposing a constant potential on the Si(*n*) electrode within the potential range corresponding to diffusion control for the deposition of gold on gold. The deposits obtained are more uniform, covering the Si surface in shorter times than with cyclic voltammetry. Their morphology is reminiscent of the surface of a cauliflower, with each grain in turn formed by smaller size grains (Fig. 8a). The grain size increases with the temperature from 150 to 193 Å. EDX analysis shows a weight percentage of 97.78% gold and 2.22% phosphorus contamination from the background electrolyte.

If deposition is performed at pH 6 a morphological change is observed, especially at high magnification (Fig. 8b). Each grain is formed by crystallites, due to the fact that charge transfer has been sufficiently fast and the

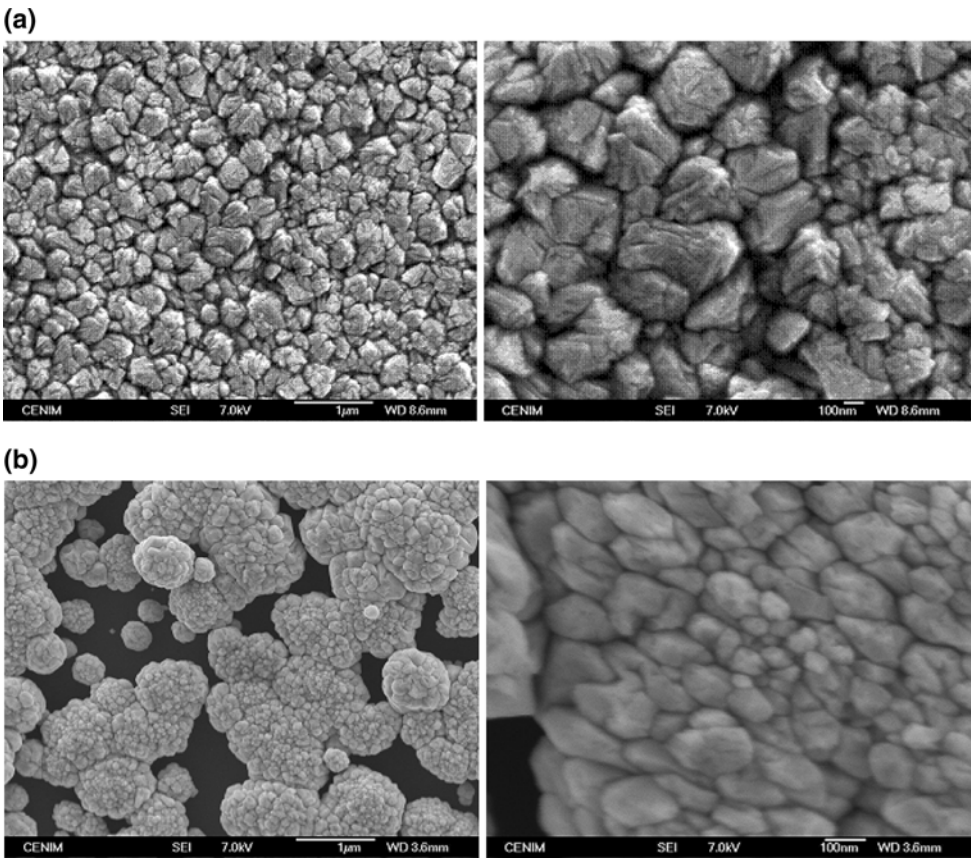

Fig. 10 Au bulk deposits on Si(*n*) obtained by constant current pH = 6, $T = 50$ °C, $t = 2$ h: **a** $I = 25$ μA cm^{-2} (DC). **b** $I = 5$μA cm^{-2} (CT). Scales 1 μm and 100 nm

ions have been reduced on the most outstanding parts of the deposit, without having time to diffuse on the surface to more energetically favourable superficial sites. Similarly, the EDX analyses show a weight percentage of 98.15% gold and 1.85% phosphorus.

The grain size obtained at constant potential for the two pH values and both temperatures is lower than that obtained by cyclic voltammetry (Table 6). Although the reduction potential is comparable in both cases, at E = cte the gold deposit does not have time to relax due to the diffusion of Au adatoms towards superficial sites with a greater coordination index.

3.2.1.3 Constant current Osaka et al. [10] studied the microstructure of gold deposits obtained at a constant current of 5 mA cm^{-2} using different $SO_3^{2-}/S_2O_3^{2-}$ ligand concentrations. They obtained columnar structures in every case with sulphur contents of between 40 and 160 ppm.

In the first place, a gold deposit was performed on Si(n) at 5 mA cm^{-2}, obtaining a granular microstructure with sulphur inclusions. The measured potential difference was several negative volts, from which it is deduced that the deposit has been formed in drastic diffusion control conditions and probably in the presence of parallel reactions such as reduction of the sulphite ion. In our case sulphur impurities are undesirable, and so the deposits have been obtained from a ligand/gold concentration ratio of 30/1 to allow charge transfer to take place without adsorbed sulphur-containing intermediates [11] and furthermore the current densities used are of the order of μA in two different regimes of charge transfer control or mass transfer control.

Figure 9 shows a gold deposit obtained under charge transfer control of gold deposition on Si(n). When reduction is a slow process, the adions have sufficient time to diffuse on the surface towards more thermodynamically favourable sites before discharging, giving rise to less rough, smoother grains. This effect increases with the temperature since the diffusion coefficient is a function of temperature (Fig. 9b) as well as the grain size (Table 6). In the same way as for constant potential, the deposition time required at constant current is shorter than with cyclic voltammetry.

Figure 10a clearly shows the effect produced by a fast charge transfer, where the exposed area for growth increases as the deposition time advances, giving rise to pointed gold grains, unlike the deposit obtained when the charge transfer is slow, where the gold grains are blunt (Fig. 10b).

The morphology obtained for a gold deposit performed at constant current when the reduction reaction of the $[Au(S_2O_3)_2]^{3-}$ complex is slow (T = 50 °C) (Fig. 10b) is similar to that obtained by cyclic voltammetry (T = 30 °C) at the same pH 6. In the case of cyclic voltammogram, the sample relaxes during a large part of the scan potential since the rate is slow and in the imposed potential range gold is only deposited at the most cathodic potentials. However, at constant current the sample relaxes its structure due to the increase in temperature. In both cases, the grain is dense and compact. Therefore, to obtain a dense, compact and smooth sample (deposit), not only is it necessary to raise the temperature and perform deposition under charge transfer control, but it is also very important that during deposition, the ions have sufficient time to reach stable sites with a greater number of coordination atoms. In this sense, deposits were performed using the square wave potential pulse technique.

3.2.1.4 Square wave potential pulse Pulsating overpotential is a periodic repetition of square overpotential

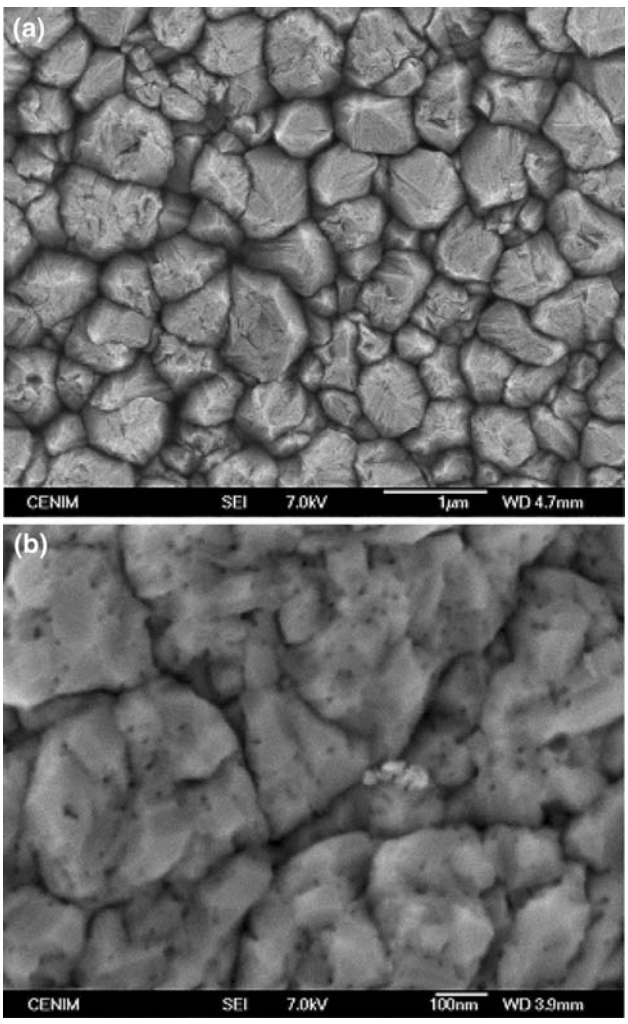

Fig. 11 Au bulk deposits on Si(n) obtained by square wave potential pulse. E_R = −0.85 V, E_D = −1.55 V, t = 6 h, pH = 9: **a** Scale 1 μm, T = 30 °C. **b** Scale 100 nm, T = 50 °C

pulses. The imposed square wave parts from an initial potential (E_R) where the sample relaxes for $t_R = 10$ ms and jumps to a final potential (E_D) where cathodic deposition takes place for $t_D = 1$ ms. The pause-to-pulse ratio ($p = 10/1$ ms) is 10, a high value to reduce the value of ω (η diffusion control/η activation) to obtain less scattered deposits [24]. In this case, stirring is not necessary, because due to the short duration of the pulse the concentration gradient on the electrode surface is very small and the initial concentration may be regenerated by diffusion during the relaxation time.

Figure 11 shows SEM images corresponding to gold deposits obtained under SWPP, giving rise to pointed grains. This fact reflects that charge transfer is so fast at −1.55 V that the ions are discharged on the outermost and least thermodynamically stable parts of the deposit. Nevertheless, the rocky appearance of the deposit is the result of superficial ionic diffusion that takes place after the discharge, since the system tends to recrystallise during the relaxation time. On the other hand, it is observed that the grain size, in the same pulse conditions, increases as the temperature rises (Table 6; Fig. 11b).

For pH 6, the relaxation potential (E_R) is changed while the deposition potential (E_D) remains constant (Fig. 12a, b), obtaining a granular structure when E_R is more cathodic. In the same way, if we maintain the relaxation potential constant ($E_R = -0.75$ V) and make E_D 100 mV more negative, the SEM image shows a deposit formed not by rounded grains but pointed grains (Figs. 12c, 13 a), since reduction is faster. Thus, it is possible to change the morphology of the deposit by changing either the deposition potential or the relaxation potential, along with the holding times in each case.

Long relaxation times give rise to an increase in the grain size, because if the system has sufficient time it tends to recrystallise to achieve a more thermodynamically stable state. An increase in the temperature has the same effect (Fig. 13). On the other hand, as in the case of cyclic voltammetry, it is necessary to apply long times to cover the electrode surface, since the average current is lower.

3.2.2 XPS analysis

In parallel with the SEM analysis of surface morphology and EDX analysis, the sample composition was studied by X-ray photoelectron spectroscopy to know what type of impurities were present and the deposited gold percentage. Gold deposits obtained by different electrochemical techniques at two pH values (6 and 9) and two temperatures (30 and 50 °C) showed similar spectra for the following elements. The high resolution C_{1s} spectrum can be resolved in two peaks: one at 284.8 eV representing carbons in a hydrocarbon environment (C–C, C–H) and the other at 286.4 eV representing carbons in a C=O bond [25]. The high resolution O_{1s} spectrum showed only a band at 532.4 eV corresponding to C=O. The presence of phosphate (P_{2p}) at 133.8 eV came from the background electrolyte. Figure 14 shows the high resolution spectrum for

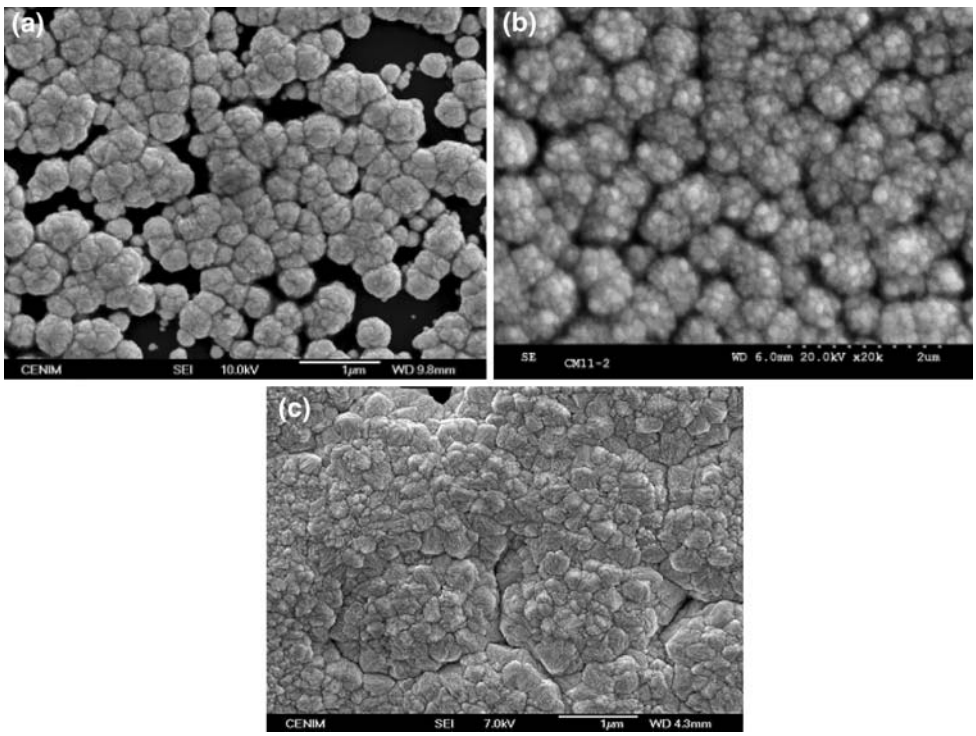

Fig. 12 Au bulk deposits on Si(n) obtained by square wave potential pulse: **a** $E_R = -0.60$ V, $E_D = -1.35$ V, Scale 1 μm. **b** $E_R = -0.75$ V, $E_D = -1.35$ V, Scale 2 μm. **c** $E_R = -0.75$ V, $E_D = -1.45$ V, Scale 1 μm, $t = 6$ h, pH = 6, $T = 30$ °C

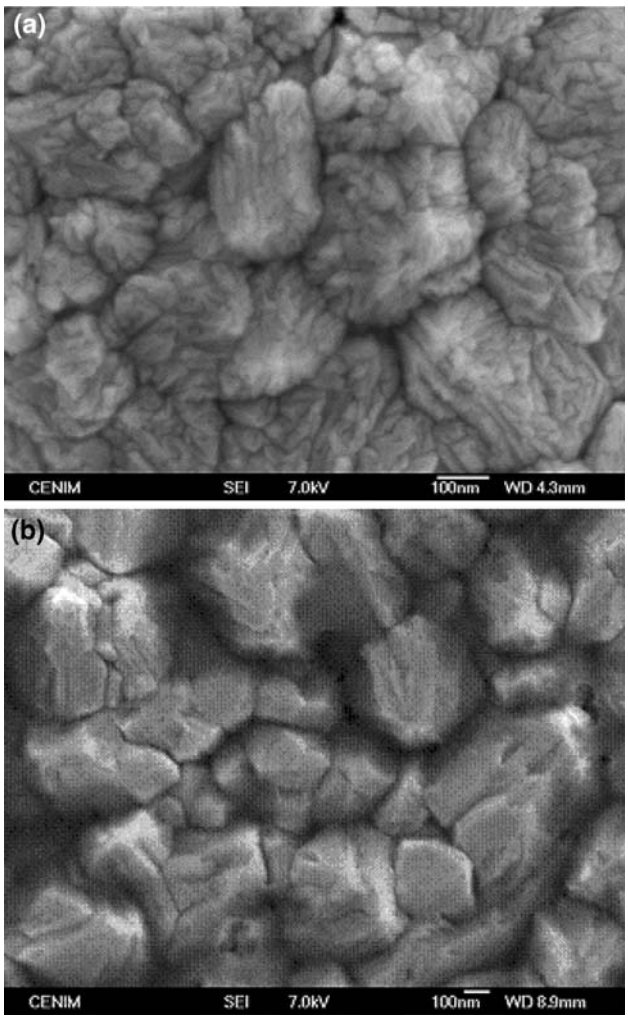

Fig. 13 Au bulk deposits on Si(*n*) obtained by square wave potential pulse. $E_R = -0.75$ V, $E_D = -1.45$ V, $t = 6$ h, pH = 6, Scale 100 nm: **a** $T = 30$ °C. **b** $T = 50$ °C

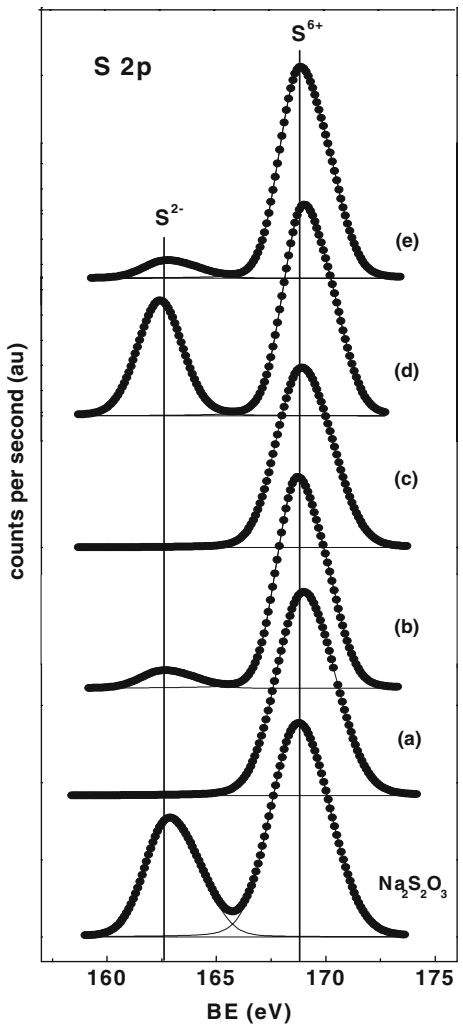

Fig. 14 High-resolution XPS of Au_{4f} and S_{2p} spectrum at the surface of: **a** $Na_2S_2O_3$, and of electrodeposited gold by different electrochemical techniques; **b** SWPP (pH = 6); **c** CV (pH = 6); **d** CV (pH = 9); **e** Constant potential (pH = 6); **f** Constant potential (pH = 9)

Au_{4f} binding energy and its deconvolution into two components: 83.8 eV assigned to metallic gold and 85.1 eV for gold partly oxidised due contact of the sample with the environment. The percentage for both is shown in Table 5. The S_{2p} spectrum showed two characteristic peaks, one at 168.6 eV corresponding to S^{+6} in the thiosulphate molecule, a component of the electrolytic bath, and a second peak at 162 eV which can be assigned to S^{2-}. In order to identify the origin of this peak, an XPS spectrum was obtained for a standard commercial thiosulphate (Fig. 14a). In this case, the S^{2-} component could be due to a S–S bond in the $Na_2S_2O_3$ sample. However, for samples obtained at pH 9 the intensity of the S^{2-} peak is much lower or almost zero compared to those obtained at pH 6. Thus, there may be a parallel reaction to gold electrodeposition at pH 6, giving rise to the presence of S^{2-}. Nevertheless, if the different methods are compared, pulsating overpotential deposition leads to the obtainment of sulphur-free gold deposits at both pH 6 and 9. Cyclic voltammetry also yields sulphur-free electrodeposits at pH 9 and deposits with a low sulphur content at pH 6, depending on the potential used. In contrast, at a constant potential or intensity the superficial sulphur content is high at pH 6 and decreases at pH 9 (Fig. 14).

3.2.3 X-ray characterization: Determination of grain size

The average Au crystallite size for Au electrodeposited was calculated by considering the line broadening of X-ray diffraction peaks by applying Scherrer's equation [26]:

$$D_{hkl} = \frac{K\lambda}{\beta \cos\theta} \times \frac{360}{2\Pi}$$

where D_{hkl} is the average dimension of the crystals in the normal direction of the planes that diffract the radiation.

Table 5 XPS binding energies of the different peak components

Sample	pH	Au_{4f}	S_{2p}
Constant potential	6	83.8 (86)	162.0 (34)
		85.2 (14)	168.8 (66)
	9		162.4 (6)
			168.9 (94)
Cyclic voltammetry	6	83.8 (68)	162.2 (8)
		84.6 (32)	168.6 (92)
	9	83.8 (77)	168.6 (100)
		85.0 (23)	
Square wave potential pulse	6	83.8 (79)	168.9 (100)
		85.0 (21)	
Constant current	6	83.8 (80)	162.0 (30)
		85.1 (20)	168.6 (70)
$Na_2S_2O_3$		–	162.2 (34)
			168.4 (66)

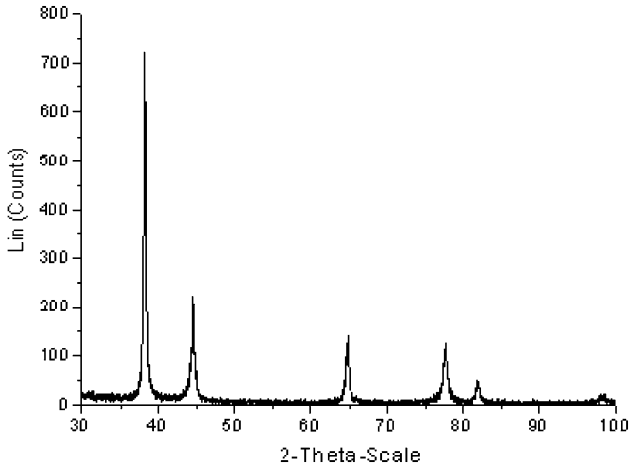

Fig. 15 XRD spectrum of a gold sample electrodeposited on Si(*n*) by constant potential at $T = 50$ °C and pH = 9 (glancing angle = 1°)

K is 0.9 when it is assumed that the particles are spherical. λ corresponds to the copper $K\alpha$ radiation wavelength. In order to make this calculation, use has been made of the weighted mean between $\lambda\alpha_1 = 1.54056$ Å and $\lambda\alpha_2 = 1.54439$ Å. β is the FWHM of the diffraction peak corrected for the instrumental broadening and 2θ the diffraction angle. X-ray diffractograms were recorded between 30° and 100° with a grazing angle to minimise the contribution of the silicon substrate.

Gold crystallises in the cubic system with $\alpha = \beta = \gamma = 90°$ and $a = b = c = 4.0786$ being the main crystallographic planes (111), (100) and (110). Calculation of the grain size for the electrodeposited gold was performed from the X-ray diffraction peak of the greatest intensity, corresponding to orientation (111). The diffractograms obtained do not show any preferential orientation and the intensities of the diffraction peaks always maintain the same relation (Fig. 15).

Table 6 Grain size in function of pH and temperature for different electrochemical methods

Method	pH	Temp	Regime	D_{hkl} (Å)
Cyclic voltammetry	9	30	CT	331
		50	CT	345
	6	30	CT	301
		50	CT	314
Constant potential	9	30	DC	150
		50	DC	193
	6	30	DC	196
		50	DC	214
Constant current	9	30	CT	255
		50	CT	282
	6	30	CT	251
			DC	199
		50	CT	267
			DC	213
Square wave potential pulse	9	30		305
		50		319
	6	30		222
		50		308

(DC) mass transfer control, (CT) charge transfer control

Table 6 presents a summary in Amstrongs of the calculated values of the grain sizes for the gold deposits obtained at two different pH values and temperatures by the application of the various electrochemical techniques used under mass transfer control (DC) or charge transfer control (CT).

The cyclic voltammetry method yields a larger grain size than the other methods, because deposition takes place at a very slow rate, and, besides, the sweep potential is mostly imposed in relaxation potentials.

It may be concluded that for any one electrochemical method for a constant pH and temperature the grain size in diffusion regime is less than if the electrodeposition process is controlled by electron transfer of the reduction of $[Au_2(S_2O_3)_2]^{3-}$ ions.

Irrespective of the electrochemical method used for electrodeposition, the grain size is larger at 50 °C than at 30 °C due, as has already been noted, to the increase in ionic diffusion with temperature both in solution and on the electrode surface.

4 Conclusions

The reaction mechanism has been determined for gold deposition on a Si(*n*) semiconductor from sulphite/thiosulphate

electrolytic baths at two different pH values (6 and 9) and two temperatures (30 °C and 50 °C), bearing in mind possible disproportion reactions of both Au^{+} and thiosulphate ions.

The Tafel slope value of 120 mV indicates that reduction of the thiosulphate complex from Au^{1+} to Au^{0} takes place through the charge transfer of an electron for a high ligand complex ratio (30/1). For lower ratios, the mechanism includes an intermediate, giving rise to deposits with sulphur content.

Measurements performed on gold substrate yield to the same mechanism but at lower overvoltages. Results obtained with the quartz crystal microbalance confirm that the reaction mechanism does not include sulphur-containing adsorbed intermediates.

Gold deposits obtained by the application of the different electrochemical techniques used, show that for a constant pH and temperature, the grain size in diffusional regime is lower than if the electrodeposition process is controlled by electron transfer of the reduction of $[Au_2(S_2O_3)_2]^{3-}$ ions.

The cyclic voltammetry method yields a larger grain size than the other methods, because deposition takes place at a very slow rate.

With square wave potential pulse, it is possible to change the morphology of the deposit by changing either the deposition potential or the relaxation potential, along with the holding times in each case.

Irrespective of the electrochemical method used for electrodeposition, the grain size is larger at 50 °C than at 30 °C due to the increase in ionic diffusion with temperature both in solution and on the electrode surface.

The constant potential and constant intensity methods yield greater coating in shorter times. However, the cyclic voltammetry and square wave potential pulse require longer deposition times since the average current is smaller.

If the different methods are compared, pulsating overpotential deposition leads to the obtainment of sulphur-free gold deposits at both pH 6 and 9. Cyclic voltammetry also yields sulphur-free electrodeposits at pH 9 and deposits with a low sulphur content at pH 6, depending on the potential used. In contrast, at a constant potential or intensity, the superficial sulphur content is high at pH 6, and decreases at pH 9.

Acknowledgements This study was supported by the Ministerio de Ciencia e Innovacion of Spain (CTQ2008-05775/BQU). We would like to thank Prof. José Luis García Fierro for XPS analysis, and C. García Alonso for giving us the opportunity to use the SEM equipment.

References

1. Stein A, Schroden RC (2001) Curr Opin Solid State Mater Sci 5:553
2. Lee K, Asher SA (2000) J Am Chem Soc 122:9534
3. Juárez BH, López C, Alonso C (2004) J Phys Chem B 108:16708–16712
4. Bartlett PN, Baumberg JJ, Birkin PR, Ghanem MA, Netti MC (2002) Chem Mater 14:2199–2208
5. Reid FH, Goldie W (eds) (1974) In: Gold plating technology. Electrochemical Publications, Ltd., Ayr, Scotland
6. Rapson WS, Groenewald T (1978) Gold usage. Academia Press, Inc., New York
7. Morrissey RJ (1993) Plat Surf Finish 80(4):75
8. Honma H, Kagaya Y (1993) J Electrochem Soc 140:L135
9. Wang X, Issaev N, Osteryyoung JG (1998) J Electrochem Soc 145:974
10. Osaka T, Kodera A, Misato T, Homma T, Okinaka Y, Yoshioka O (1997) J Electrochem Soc 144:3462
11. Osaka T, Kato M, Sato J, Yoshizawa K, Homma T, Okinaka Y, Yoshioka O (2001) J Electrochem Soc 148:C659
12. Green TA, Liew MJ, Roy S (2003) J Electrochem Soc 150:C104
13. Oskam G, Searson PC (2000) Surf Sci 446:103
14. Oskam G, Searson PC (2000) J Electrochem Soc 147:2199
15. Huang Q, Deligianni H, Romankiw LT (2006) J Electrochem Soc 153(5):C332
16. Depestel LM, Strubbe K (2004) J Electroanal Chem 572:195
17. Garcia-Alonso C, Escudero ML, Alonso C (2008) Pat. No. 200801041
18. Wagner CD, Davis LE, Zeller MV, Taylor JA, Raymond RH, Gale LH (1981) Surf Interface Anal 3:211
19. Pourbaix M (1966) In: Pourbaix M (ed) Atlas of electrochemical equilibria in aqueous solutions. Pergamon Press, London
20. Bard AJ, Faulkner LR (1981) In: Bard AJ (ed) Electrochemical methods, fundamentals and applications. Wiley, New York
21. Sauerbrey GZ (1959) Phys 155:206
22. Scharifker B, Hills (1983) Electrochim Acta 28:879
23. Scharifker B, Mostany J (1984) J Electroanal Chem Interfacial Electrochem 13:177
24. Popov KI, Masimovic MD (1989) In: Conway BE, Bockris O'M, White RE (eds) Electrochemistry, vol XIX. Plenum Press, New York, p 193
25. Moulder JF, Stickel WF, Sobol PE, Bomben KD (1992) In: Chastain J (ed) Handbook of X-ray photoelectron spectroscopy. Perkin-Elmer, Eden Pranic
26. Cullity BD (1978) Elements of X-ray diffraction, 2nd edn. Addison-Wesley Publishing Company, Reading, p 284 Ch 9